Novel device for determining the effect of jetting shear on the stability of inkjet ink

Patrick A.C. Gane[1,2]*, Monireh Imani*[1]*, Katarina Dimić-Mišić*[1] *and Enn Kerner*[3]

[1] School of Chemical Engineering,
　Department of Bioproducts and Biosystems, Aalto University,
　00076 Aalto, Helsinki, Finland
[2] Faculty of Technology and Metallurgy, University of Belgrade,
　Karnegijeva 4, 11200 Belgrade, Serbia
[3] International Circle of Educational Institutes for Graphic Arts,
　Technology and Management (IC) / Grafitek, 13512 Tallinn, Estonia

patrick.gane@aalto.fi
monir.imani@aalto.fi
katarina.dimic.misic@aalto.fi
enn@trykitehno.eu

Abstract

Inkjet printing is a rapidly expanding technology for non-contact digital printing. The focus for the technology has changed from office printing of text and image documents increasingly toward wider applications, including large-scale printing of on demand books and packaging or ultra-small-scale functional printing of microscopic volumes of precious/rare materials formulated for use in precisely printed digitally defined patterning arrays, such as printed diagnostics, flexible electronics, anti-counterfeiting, etc. For efficiency, as well as resource management and conservation, predicting the stable runnability of an inkjet ink remains largely a key unknown. Today the only way to know often means simply trialling it, which at best takes time, and at worst incurs costs rectifying possible equipment damage. We propose a mechanically driven displacement device providing constant high-shear flow rate through an extended capillary. This differs from a standard capillary viscometer, which is commonly pressure driven only and lacks the ability to mimic consistent volume flow inkjetting. The novel method is used to study the aqueous colloidal stability of polymer solution, latex polymer suspensions and complete pigment-containing inks, including a reference pigment only comprising suspension. The results reveal the tendency to build agglomerates, determined by dynamic light scattering particle size distribution, optical and electron microscopy. Liquid phase parameters, including surface tension, and suspension intrinsic viscosity are also studied. Repeated application of high shear is seen to act as a milling process for pigment and agglomerate building tendency for latex binder. Consequences for ink jettability are discussed.

Keywords: ink jettability, ink stability, nozzle blocking, shear-induced aggregation, ink flow testing

1. Introduction and background

Non-contact printing has developed hand-in-hand with the digitisation of text and images, commonly seen in everyday life during the boom era of office printing. Compared with traditional contact printing dating from letterpress through to high-speed offset, flexography and rotogravure, non-contact digital printing, whilst having shown a dramatically rapid development timescale, has had a working lifetime that is extremely short in terms of conveying the written word, and document printing in general is declining rapidly in the face of electronic media. However, its longevity cannot be challenged when it comes to print-on-demand applications and for advanced functional printing, such as flexible electronics, microfluidic point-of-care diagnostics and repetitive laboratory analytics, building biological structures, including tissue and protein cages for constructing human organs and implants, photonic and photovoltaic coatings, etc., enabling complex designs to be formed from low volume availability functional materials (Alamán, et al., 2016; Beedasy and Smith, 2020; Cui, et al., 2012; 2014; Eggenhuisen, et al., 2015; Gao, Li and Song, 2017; Jiang, et al., 2019; Jutila, et al., 2015; 2018; 2020; Kim, et al., 2009; Koivunen, Jutila and Gane., 2015; Koivunen, et al., 2016; 2017; 2019; Matsusaki, et al., 2013; Saarinen, et al., 2014; Sumaiya, Kardel and El-Shahat, 2017; Zönnchen, et al., 2019).

Amongst the array of non-contact digital printing platforms, inkjet offers a broad spectrum flexibility in respect to the printing of small quantities of valuable materials on multiple substrates, a feature that is particularly important in the laboratory and in mass production of components employing functional materials.

Before considering the complexities of the inkjet printing dynamic itself it is perhaps important to remind ourselves briefly of the preparation of an inkjet ink. A typical recipe for an aqueous ink might comprise of:

Solvent 1: ~20 % in the ink; the major part is water (demineralised water, millipore water)

Solvent 2: ~20–35 % in the ink; consisting typically of glycerine, diethylene glycol, polyolefin glycols, such as polyethylene glycol (PEG) and polypropylene glycol (PPG) in small proportions

Surfactant: ~0.02–1 % in the ink; usually non-ionic to prevent disturbance of the anionic stabilising colloidal dispersion system

Binder: ~10 % in the ink; mainly acrylic resins, and considered a very challenging material component in the form of synthetic latex – acts as fixing agent, and is considered perhaps to have the biggest influence on jetting failure

Pigment: ~5 % of the total ink weight if used in preference to dyes, and controls optical and physical properties – dot shape and volume during dewatering and after drying, light absorption and scattering properties; the pigments formulated into inkjet inks are typically dispersed to small particle sizes (between about 50 nm and 200 nm, depending on the application) and need to be colloidally stable in suspension

Humectant: sorbs moisture from the surrounding atmosphere, used to prevent ink drying around printhead plate, nozzle and in recycling (continuous inkjet)

Buffers: to control pH

Biocide: acts to preserve the ink from microbiological contamination

These components are prepared and "madedown" into the ink following a sequence similar to that shown in Figure 1.

Premix
Stabilisers, dispersants, humectants, binder(s) and fixatives are added with pigment(s) and/or dyes to develop colour, rub fastness, light fastness and drying/fixing characteristics

Predispersion
Agitation and shear are applied to disperse the pigment initally at high solids content in water and/or solvent (aggregates and inhomogeneities remain)

Grinding and milling
Refining the predispersed mix to breakdown aggregates and decrease pigment particle size – improves colour intensity and homogeneity, benefiting print uniformity, surface strength and fixing

Flow properties control
High solids ink is diluted to achieve desired viscosity and dispersion maintained under slow agitation
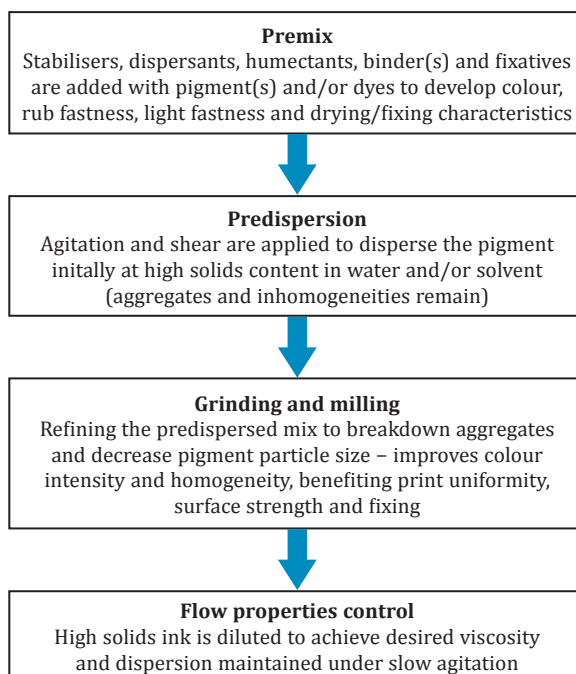
Figure 1: Schematic procedure for makedown of a typical pigment-containing ink
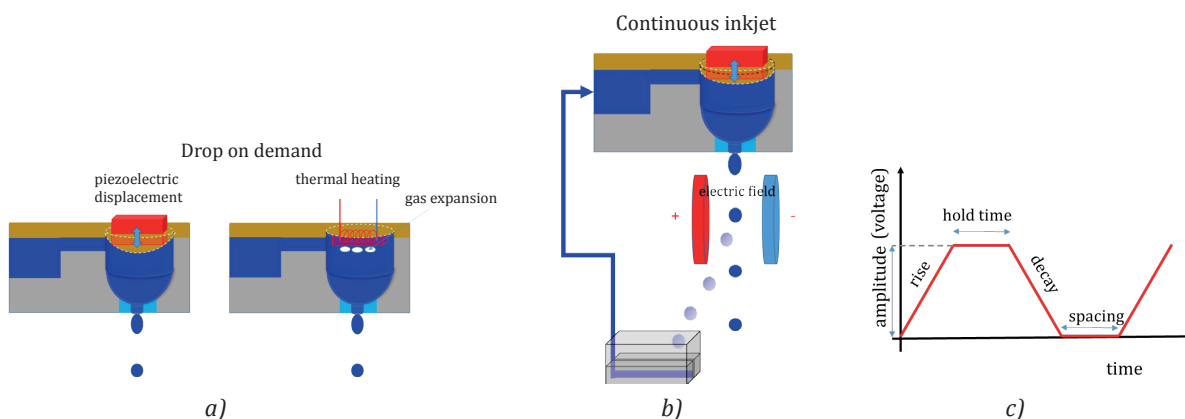

Figure 2: Inkjet technologies commonly used: (a) drop on demand, driven typically either by piezoelectric displacement or heating to expand gas bubbles, (b) continuous inkjet, where the droplets are jetted repetitively and directed either toward the substrate or to recycling via a collecting trough; and (c) an idealised activator voltage waveform

Despite the many advantages that inkjet technology provides, the technique can be marred by runnability-limiting phenomena depending on the nature of the technology itself. As we can see from the schematic of an inkjet printhead, Figure 2, the process is highly dynamic and the forces needed to jet ink are confined within a very small volume.

As we see from the voltage waveform in Figure 2c, the ink is subjected to rapid acceleration and deceleration in response to the applied activator voltage amplitude rise and decay time, repeated consecutively according to the time spacing. This causes the ink to be forced through a narrow nozzle during the voltage hold time, as shown in Figure 2, where the flow regime may be discontinuous between inertial boundary solids depleted plug flow and high-shear viscous flow. For drop on demand the repeated compression and inertial response of retained bulk ink in the ink chamber is experienced many times before the critical ejection through the nozzle, and has been evaluated, at least partially, using exit meniscus imaging in terms of viscoelastic response (Renner and Bircher, 2017), whereas in continuous inkjet the same demanding regime is applied not for one filling of the chamber, but many times as the ink is jetted, fed back to the chamber, exposed to repeated inertial pulses and then jetted again with the possibility of being recycled repeatedly, even when printing has stopped in order to keep the ink in the nozzles from drying and blocking. To bring this into perspective, high-speed jetting is achieved typically by applying a high frequency (~100 kHz) to the piezoelectric displacer, this displaces a volume commonly down to 6 pl (picolitres) – and in more recent times even as small as 2 pl – at 1 200 dpi for controlled ejection per droplet, translating to a rate of 6 million drops per minute, all leading typically to an ink consumption of up to 12 dm^3 per hour printing at a substrate surface traverse speed of 6–15 m·s^{-1}. Today's ink manufacturers additionally aim to minimise the wetting effect on fibre-based substrates. The more the ink wets and becomes absorbed between and within the fibres, the more the energy needed to dry the ink, and, depending on ink film thickness and the time taken to dry, the droplets can spread undesirably on the substrate surface. This development target promotes further the desire to reduce ink volume, and it is this precision and small volume content applied at high speed that makes the flow regime for the ink highly complex.

It is vital to prevent damage to the printheads caused by changes in the ink over time under such conditions as described above. Should an ink form dry deposits or cause nozzle blockage, the printhead requires cleaning. Experience, though, tells us that cleaning agents are also a suspected culprit in leaving deposits and do not generally work well.

Other runnability-limiting phenomena also exist, such as over-wetting of the nozzle exit or air ingress and entrainment inside the exit, leading to ink build-up around the nozzle and housing plate, resulting, in turn, in droplet volume and trajectory distortion. Humectant is used to retain water in aqueous inks to act against such nozzle build-up and blockage due to evaporation and drying.

The work reported here is not aimed at addressing the whole multiplicity of runnability issues, rather it concentrates on the suspension stability as a response to jetting at high shear, which is primarily responsible for suspension solids-related nozzle blocking (for example: Biswas, Yu and Nierstrasz, 2019; Ebert, et al., 2009; Lee, et al., 2012; Li, et al., 2019; Wheeler, et al., 2014), and resulting in uneven dot distribution and lack of circularity of the printed dot, especially noticeable on smooth non-absorbing substrates. Furthermore, variation in print and colour density parameters, independent of substrate, are often due to inhomogeneous distribution on the surface and contrast between dispersed pigment, flocculated pigment and aggregated pigment. We aim, therefore, to provide some answers to the question: "How can we know an ink works in practice before using it?" Today, the only way is to try it and see.

2. Methods

Here we address why there is the need for a new technique in determining relevant inkjet ink flow behaviour away from the printer itself, and present the ancillary testing methods employed to analyse the results obtained from a constant flow rate device using carefully chosen materials.

2.1 Traditional rheometry – lack of suitability for inkjet

Measurement techniques for determining the rheological properties of liquids and suspensions are historically well established, and based primarily on the analysis of the stress developed in the sample as a function of applied strain. Many geometries and diverse methods for applying strain are available. Two dominant methods exist, (i) consisting of a means of containing the sample under constant volume within a uniform set of boundaries, then coupling one boundary with a driving mechanism to generate controlled displacement as a function of time with a sensor to detect the coupling of the displacement to transmitted stress, and (ii) pressure-driven extrusion through a capillary or slot to observe the volume flow rate as function of pressure and time. In (i) the displacement can be linear, giving a dynamic shearing effect on the sample, or

oscillatory, providing a continuously variable strain amplitude oscillation at a determined frequency, the latter being particularly useful in measuring the viscoelastic response of materials exhibiting a rest-state or strain-induced structure. Rotational instrumentation is accordingly commonly used to study oscillatory behaviour, and when controlled by electronic feedback can also be used as a continuous measure of viscosity under controlled internal stress without applying oscillation. Method (ii) is primarily reserved for observing liquid behaviour under very high shear rates, which can also reveal die-swell behaviour at the exit from the capillary and so including the ability to estimate elastic behaviour. Less commonly used, but nonetheless relevant, (iii) extensional geometry can be used. Essentially, a sample, typically a polymer melt or solution is rapidly extended as a filament under controlled rate, and the thinning to breakage of the filament recorded to reveal a resistance to extension as an extensional viscosity. Combining shear rate, as the rate of change of stress within the sample within these various methods, the material viscosity can be derived (Whorlow, 1992).

The techniques described above are regularly applied to coating suspensions, including printing inks (Hoath, et al., 2009; Tuladhar, 2017; Vadillo, et al., 2010a; 2010b; Yokoi, et al., 2009). Traditional printing technology submits inks to flow, strain and extension in regions of pumping, transfer, film splitting, etc. The ink properties determine its resistance to these applications of strain and extension, and of particular interest is the change of these properties over time. Method (i) in rotational controlled stress mode is an ideal tool to provide "day zero" quasi quality/consistency control information about an inkjet ink before use.

In the case of inkjet in the print application, the ink is either delivered to the substrate as a droplet on demand or as a deflected pathway choosing whether to accept an ejected ink droplet within a continuous stream of such droplets or reject it according to the image requirement. The mechanism used to create the droplet, however, differs fundamentally from those processes familiar in traditional printing methods, such as offset, flexography or gravure. Inkjet technology applies a displacement to the incompressible liquid ink, either via a fixed-response piezoelectric element or a heating device used to expand the ink or a gas bubble within it. The end result is to meet the requirement of extruding a fixed volume of ink from a capillary-like nozzle independent of the ink's rheological properties, which must lie within a given range for the technique to function correctly. The shear rate under these conditions is typically ~10^5 s^{-1} to 10^6 s^{-1}, and, by nature, the applied strain is in the form of a pulse, which can be controlled in terms of ampli-

tude, waveform, and dwell time between each pulse. This force, time and geometrical constriction used to provide a fixed droplet volume thus determines the difference between digital inkjet and classical analogue print technologies, i.e. inkjet is fixed-volume, displacement-driven, whereas traditional printing is ink-responsive pressure-driven. Thus, we see that the method (ii), namely pressure-driven capillary viscometry, fails to replicate the inkjet mechanism designed to deliver a fixed volume in a given time. Why this is the case, is worth discussing in a little more detail.

Capillary viscometry relies on the Hagen-Poiseuille relationship for flow in a pipe

$$Q = \frac{\mathrm{d}V}{\mathrm{d}t} = \frac{\pi R^4 \Delta P}{8\eta l} \qquad [1]$$

where Q is the volume flow rate $\mathrm{d}V/\mathrm{d}t$ of a liquid, having viscosity η, through a cylindrical pipe (capillary) of radius R and length l under an applied pressure difference of ΔP. The observed flow rate is, therefore, responding to the pressure applied as a function of its viscosity. This situation would be useless in inkjet as the flow rate must be a constant. In other words the pressure must rise to the necessary value to extrude a fixed volume of ink in a given time. This can only be achieved using a displacement pump rather than, for example, a gas overpressure. We are forced, therefore, to abandon classical capillary viscometry and design a displacement-driven apparatus to be able to expose an inkjet ink experimentally to the high-shear conditions experienced in application.

2.2 Instrument design – positive displacement

Our design for the experiment is shown in Figure 3. A motor-driven piston expels the ink from a cylindrical syringe and forces it to flow at high shear rate through a capillary. The ink is collected, drawn back into the syringe and so passed a controlled number times repeatedly through the apparatus. A sample can be collected after passage through the capillary and analysed for any change in suspension particle size, surface tension and its intrinsic viscosity. Particle size change is sensitive to particle dispersion state, such as the state of any suspending colorant pigment and/or particulate latex binder, i.e. it reveals flocculation or agglomeration induced by the mechanical stress by showing an increase in size, or the contrary in the case where the induced stress might have actually broken-down any pre-existing structures. Intrinsic viscosity, measured as the flow time required for a given volume of ink to flow through a capillary restriction under gravity (low shear) reveals additionally the condition of any polymer content in relation to the suspension, i.e. a drop in intrinsic viscosity reveals a breakdown in polymer chain length, or it matches the breakdown of sus-
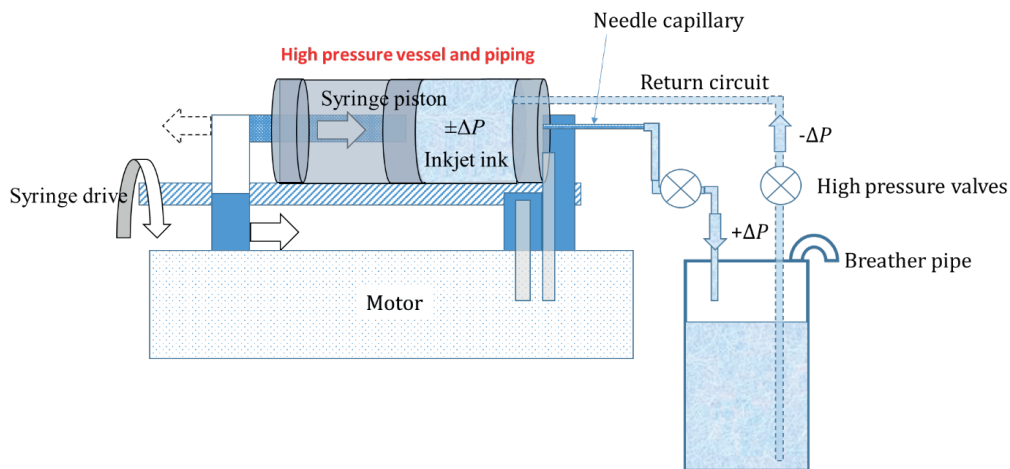
Figure 3: A schematic representation of the experimental apparatus design used to mimic the fixed displacement condition of an ink-jetting process

pension agglomerates, whereas an increase reveals polymer entanglement of structure build within the suspension.

Such polymers exist, for example, as dispersing agents, such as the frequently used polyacrylate dispersant in aqueous inks for ensuring colorant pigment colloidal stability and binding to the substrate, being soluble in the sodium form but precipitated in the calcium form, and, hence, particularly sensitive to contact with divalent alkali metal ions. Other polymers are present frequently as viscosifying agents, humectants, surfactants or as oligomer and monomer residues in latex binder product suspensions. The free polymer content, in particular the presence of surfactant, defines the surface tension of the ink, and any changes to the surfactant itself, or its concentration, that might occur during jetting can be monitored by measuring the surface tension, σ.

The apparatus as installed in the laboratory is shown in Figure 4, and the extrusion of liquid (water in this case) from the capillary and the return flow system is shown in Figure 5.
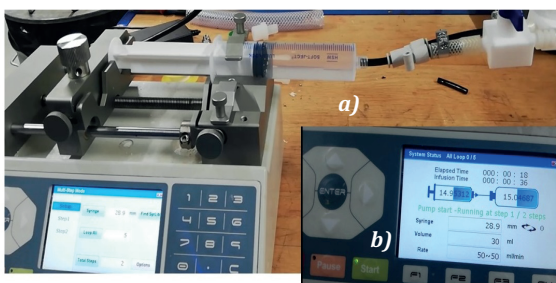

Figure 4: (a) Syringe and motor drive connected to the capillary via a valve, also showing the return flow junction element, (b) motor speed drive controller
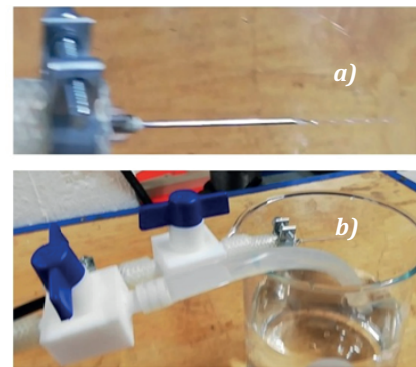

Figure 5: (a) Liquid extruding from the capillary at high speed, (b) return pipe and connection valve system for multiple passes through the syringe

To prevent contamination of the sample a number of precautions needed to be taken. The liquid collection vessel needed to be covered under a sealed film. Sampling was made by mechanical pipette, and each pipette sealed for transportation (Figure 6) to the nearby enclosed laboratory area to perform particle size and intrinsic viscosity analyses – subsections 2.4 and 2.5, respectively.

Figure 6: Taking care to isolate samples from contamination using a mechanical sealed pipette, transported in a film-sealed vessel

2.3 Flow analysis

To enable the analytical flow conditions to be determined, the following theoretical background needs to be considered.

Flow rate Q through a capillary is given, as we saw previously, by the Hagen-Poiseuille equation, Equation [1]. Whilst flowing through, the shear rate $\dot{\gamma}$ experienced by the liquid is given by

$$\dot{\gamma} = \frac{4Q}{\pi R^3} = \frac{\left(\frac{4\pi R^4 \Delta P}{8\eta l}\right)}{\pi R^3} = \frac{R\Delta P}{2\eta l} \qquad [2]$$

Thus, the parameters to be adjusted to achieve the desired shear rate at the resulting system flow rate Q are R, l and ΔP, so as to arrive at the representative shear rate of $10^5 \lesssim \dot{\gamma} \lesssim 10^6$ s^{-1}. By finding a conveniently suitable fine capillary, such as used typically in a high shear capillary viscometer, and so knowing R and l, it is then possible to design for the required pressure by displacement.

To calculate ΔP in a syringe one must consider the pressure drop across the capillary, which is given by the Bernoulli expression, and the relationship of pressure to the speed of the syringe piston displacement. The velocity at the end of the capillary, v_2, is given by the ratio of the cross-sectional areas of the syringe A_1 and capillary A_2 ($= \pi R^2$) given the velocity before the capillary, v_1, which is the speed of the syringe piston

$$v_2 = v_1 \left(\frac{A_1}{A_2}\right) \qquad [3]$$

Applying this in the Bernoulli formula gives us,

$$\Delta P = \rho(v_1^2 - v_2^2) \qquad [4]$$

which is negative, as it is a pressure drop, where ρ is the liquid density, and $v_2 = Q/\pi R^2$.

This then leaves us with the answer from Equation [3] of how large the syringe diameter ($D^2_{\text{syringe}} = 4A_1/\pi$) must be in combination with the adjustable speed of the piston. The piston activator is more controllably run at a slow rate.

Using the equations above we chose the following parameters to work with. A mechanical syringe was chosen that delivers 50 cm^3·min^{-1} (i.e. $Q = 50 \times 10^{-6}/60$ m^3·s^{-1} = (5/6) × 10^{-6} m^3·s^{-1}).

We need a shear rate up to $\dot{\gamma} \sim 10^6$ s^{-1}. From Equation [2] we can, therefore, calculate the capillary radius required $\left(R = \sqrt[3]{4Q/(\pi 10^6)}\right) \approx 0.1$ mm, i.e. a capillary diameter of 0.2 mm.

To provide a sufficiently extended period of shear in order to reduce the number of passes needed to obtain a result, a convenient capillary length of 40 mm was chosen. The pressure drop along the capillary length, is then given from Equation [1] as $\Delta P = 47.21 \times 10^3$ Pa, which is approximately equivalent to 0.5 bar. However, in this experimental design it is extremely important to recall that the system is running under constant flow rate, such that the pressure build-up can rapidly increase should there by a blockage or an increase in viscosity either by using a different liquid ink or by an ink that shear thickens – rare but not negligible possibility –, i.e. instead of the case of a normal capillary viscometer, where $Q \propto \Delta P/\eta$, the situation here is a constant displacement apparatus, such that $\Delta P \propto \eta$, which means that a factor increase in viscosity is directly raising pressure by the same factor.

Therefore, it is very important to make the calculation as to what the pressure is likely to be, so that the apparatus is run safely in respect to the material construction. For safety reasons a pressure release valve and/or motor power cut-off sensor should be fitted, and if the liquid properties are not known beforehand, then a protective cover should be installed to contain liquid should there be a vessel or piping failure. Additionally, also pressure-related, the capillary should always point into a receptacle or toward blocking material, in case it should blow out and cause injury. One other non-safety-related issue is to avoid the ingress of air bubbles into the system, as these act to reduce the condition of constant flow rate as the air compresses, and air in ink can also lead to internal drying at the bubble interface, resulting in solids contamination as well as potential oxidation.

2.4 Particle size measurement

Microscopic particles in suspension undergo Brownian motion, which is observed as a translational diffusion rate through the liquid medium using the autocorrelation function over time of the real time varying dynamic laser-light scattering intensity $I(t)$. The decay of the autocorrelation function provides the translational diffusion rate of the particles. This, in turn, is inversely proportional to the ensemble average equivalent spherical diameter (*esd*) of the particle moving at that diffusion rate through the liquid according to the Stokes–Einstein relation

$$esd = \frac{k_B T}{3\pi \eta_{\text{liquid}} D_{\text{translation}}} \qquad [5]$$

where k_B is Boltzmann's constant, T the absolute temperature, η_{liquid} the suspending liquid phase dynamic viscosity, and $D_{\text{translation}}$ the translational diffusion coefficient determined from the e-folding decay Γ of the light scattering autocorrelation function,

$$\int_{\tau=0}^{\infty} \frac{I(t)I(t+\tau)}{I^2(t)}\, d\tau = e^{-\Gamma\tau}$$

$$D_{\text{translation}} = \frac{\Gamma}{\left(\frac{4\pi n}{\lambda}\sin\frac{\theta}{2}\right)^2}$$ [6]

in which n is the refractive index of the particulate material in the suspending liquid, λ the wavelength of the laser light, and θ the angle from the axis at which the scattering is recorded as a function of time, τ. By using multiple iterative deconvolution of the auto-correlation function, supported by software, a particle number size distribution (in %) can be obtained (Zetasizer, Malvern Instruments, UK).

It is important to recognise, as described above, that the particle size data in this study are reported as particle number distributions, based on the scattering volume occupancy effect of each particle in the suspension, which naturally skews the results toward the larger number of finer particles per unit mass of material compared with coarser ones. This differs from most industrial representations, which use individual particle mass concentration, which naturally skews the data toward the coarse particle range. We chose this representation on purpose, so that visual assessment of larger scale agglomeration can be directly compared with optical and electron microscopy. The finer scale structuration, in particular, can be well investigated using the higher resolution of electron microscopy.

2.5 Intrinsic viscosity

The low-shear flow of the ink before and after passage through the displacement pump and capillary was measured as the time taken to flow through an Ostwald glass viscometer, as shown schematically in Figure 7.
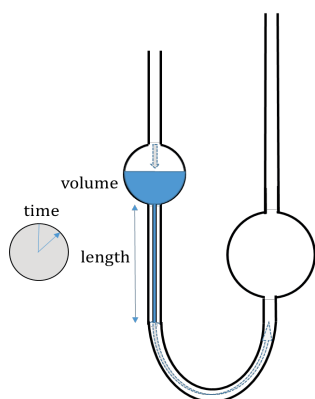

Figure 7: Ostwald viscometer for measuring intrinsic viscosity – time for liquid to pass via the thin capillary restriction is a relative measure of low-shear intrinsic viscosity

The intrinsic viscosity reveals the volume fraction effect of the suspended or dissolved content. Thus, the response of the intrinsic viscosity of the samples to repeated jetting shear reveals the nature of structural elements, as shown schematically in Figure 8, in which a highly dispersed system "day zero" with repulsive interaction manifests a given rest state viscosity, a dynamically induced packing change can result in a higher volume fraction swept out by flocculated particles or coiled polymer, and finally a strongly aggregated material acts as a fewer number of now coarser particles, and, hence, represent a reduced interactive volume fraction.
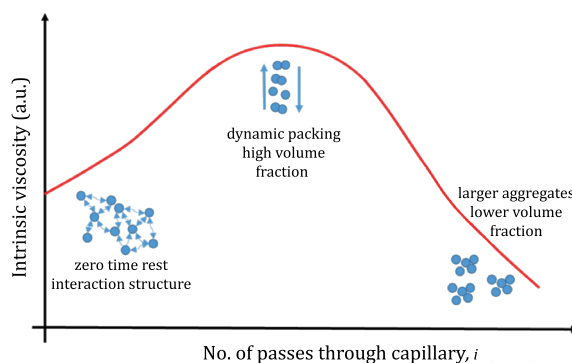

Figure 8: Schematic of the effect of different packing interaction states on intrinsic viscosity

For common ink usage, it is sufficient to follow the typical printhead manufacturer's advice for ink viscosity under these conditions, commonly within the range from 4 mPa·s to 9 mPa·s.

2.6 Surface tension

Ink behaviour when exiting the nozzle and spreading on the printhead plate, as well as wetting the substrate, depends on surface tension (Krainer, Smit and Hirn, 2019). Liquid surface tension can be measured from a bulk liquid sample using the du Noüy ring method. A thin ring of known circumference, typically made from platinum, is lowered into contact with the planar surface of the sample liquid and subsequently slowly raised to form an extended meniscus.

The force F_σ required to raise the ring against the action of the liquid surface tension, corrected for the weight of the ring itself, is related to the surface tension via the length of the contact line on both the inner and outer surface of the meniscus adhering to the ring, namely,

$$\sigma = \frac{F_\sigma}{2\pi D_{\text{ring}}}$$ [7]

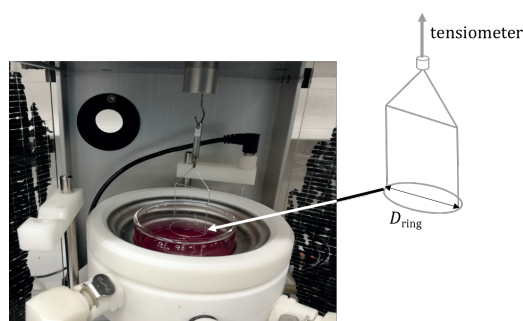where D_{ring} is the diameter of the ring used, Figure 9.

Figure 9: Surface tension measurement
using a du Noüy ring tensiometer

2.7 Materials

The materials were collected as best for purpose as could be achieved, given the ubiquitous difficulty of sourcing information on commercial products. The design of sample choice we desired was, nonetheless, more or less catered for, in that we first set out to determine if the experimental concept would actually act out correctly upon trial materials successfully. Therefore, starting with a simple polymer, known to break down under the print dynamic in inkjet, enabled us to gain confidence in the suitability of the test concept (Wheeler, et al., 2014). Once demonstrated, then the task was to move on to the separate components of binder and pigment. Latex binders were suitably acquired by the co-author team and others donated after much searching by a helpful manufacturer's R&D group. Inks proved equally difficult to find, but thanks to one co-author (EK) three "inks" were provided, two based on a couple of the acquired latices and one a "reference" ink comprising a commercial inkjet water-based ink for high-speed digital printing (web speed up to 150–200 m·min⁻¹). The reference ink was developed in cooperation with one particular printhead manufacturer to be suited especially for such extreme rheological conditions.

2.7.1 Polymeric constituents – polyvinyl alcohol and latices

To establish some prior knowledge of the effect of jetting shear on polymeric components of ink, two typical polymer molecules and compound types were studied

individually, namely a polymer solution of polyvinyl alcohol (PVOH, MOWIOL® 4-88, M_w ~31 000, Sigma Aldrich), and four latex compound binders. The latex binders were supplied as aqueous dispersions. Two of the latices were formulated by the manufacturer with and without urethane modification (Acrycote® anionic styrene acrylic emulsion AP-600 K and urethane modified AP-600 K-1, supplied by APEC Ltd. R&D Centre, Republic of Korea). Since the AP binders were, respectively, a commercial product and a modified commercial product, necessarily no further detailed information on their polymerisation or manufacture could be divulged by the supplier. The further two latices came from non-disclosable origin, and so are labelled as L1 and L2. In the interests of understanding changes in chemical composition as a function of jetting, all the latex samples were analysed using Fourier transform infra-red (FTIR) spectroscopy (PerkinElmer, Finland Oy) before and after shearing by forming dried films. The films were made by pouring a thin layer of suspension in a Petri dish and then drying at room temperature (25 °C). Flakes of the films (Figure 10) were used for the spectroscopic analysis and yielded spectra as shown in Figure 11.
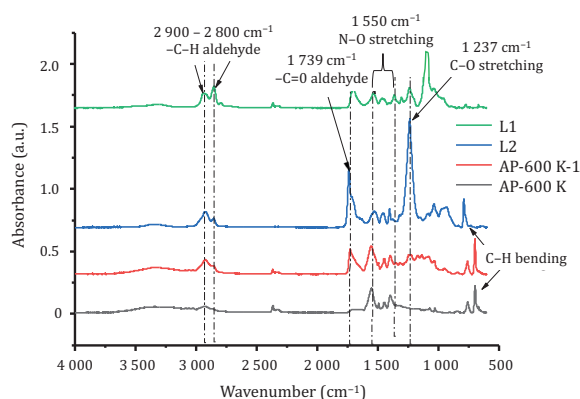

Figure 11: FTIR spectra of the latex binders –
the units of absorbance are arbitrary
and the stacked spectral plots
are of comparable magnitude
(processed by spectrum software,
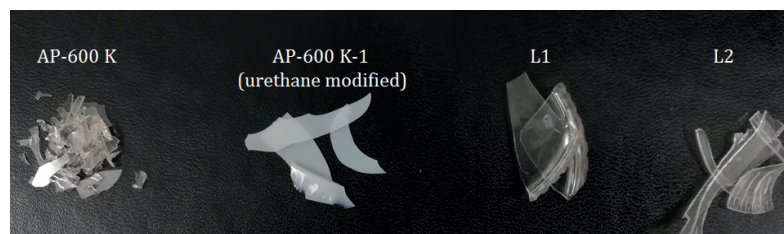*PerkinElmer v. 6.3.5)*

The latex binders are described in Table 1.

Figure 10: Flakes of dried latex films as used for FTIR analysis

P.A.C. Gane, et al. – J. Print Media Technol. Res. – Vol. 10 No. 1 (2021), 7–24

15

Table 1: Available details of as-supplied and experimental preparation of latex binders

Latices	Initial mass fraction (%)	Mass fraction prepared for passes through capillary pump (%)	Initial pH (as supplied)	Corrected pH for passes through capillary pump
AP-600 K	10.65	5	8.10	8.10
AP-600 K-1	23.43	5	8.25	8.25
L1	36.60	5	7.78	8.35
L2	35.23	5	8.40	8.30

The solids content and pH were adjusted, using deionised water and 0.1 M NaOH, respectively, to represent their solid mass fraction properties present in an ink, typically 5–10 %.

2.7.2 Inkjet inks – complete formulation

Following the analyses of the single components, three commercial pigment-containing ink formulations were tested, which, once again for proprietary reasons, are represented as inks A, B and R from a printing house, where R was termed as the reference ink. Inks A and B, by contrast, were formulated trial inks containing latex L1 and L2, respectively. For these materials little is known about other formulation additives, however since the exercise in the study reported here is to investigate if a method of applying representative jetting shear can reveal characteristics of ink stability/instability, the detailed knowledge of their makeup is, fortunately, less relevant than their generic character. The formulated inks are now in current industrial use, and so can be considered relevant. Table 2 shows the as-delivered solids content of the three inks.

Table 2: Ink solids contents

Ink	Solids mass fraction (%)
A	23.86
B	23.43
R (reference ink)	31.72

2.7.3 X-ray photoelectron spectroscopy

By studying the atomic elemental content using X-ray photoelectron spectroscopy (XPS) the changes in the composition of the surface layer of the ink and influence of shearing after several passes were determined.

3. Results and Discussion

We begin by considering the results from the application of multiple passes of the single component materials, starting with the water soluble PVOH used to

determine if the shear regime is sufficient to cause polymer breakage or coiling, as would be expected from the prior-art experience of inkjet printing polymer solutions (Wheeler, et al., 2014). Results from the four latex suspensions are considered in detail, followed by the inks A and B, containing each of them (L1 and L2), respectively, in comparison with the "reference" ink R.

3.1 Polymer breakdown of PVOH in solution under shear

PVOH solution is a typically used adhesive binder in coating formulations. Solubility is controlled by molecular weight and level of hydrolysis, both inversely. Figure 12 shows the effect of increasing number of passes through the pump syringe capillary, where it can be seen that after a low number of passes the polymer chain gel network properties of the polymer at a concentration of 5 000 ppm have been broken down. This structure (Figure 12a) does not rebuild, even after many hours, i.e. the time between shearing, collecting the samples and measuring their intrinsic viscosity.
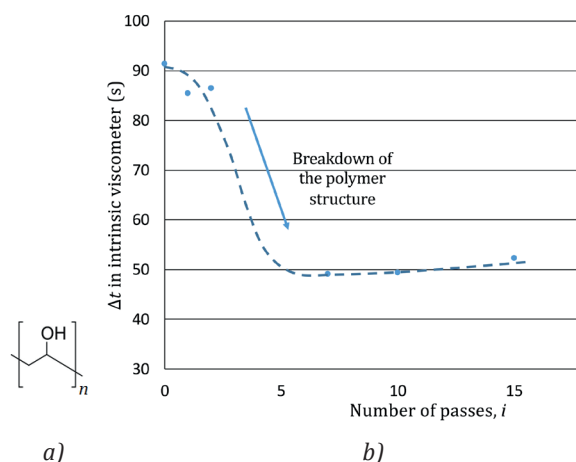
Figure 12: a) PVOH and b) the impact of repeated jetting shear on instrinsic viscosity time interval of PVOH solution (5 000 ppm) – the dashed line is to assist the eye to follow the trends, and could form the first approximation to an experimental function describing the curve

Thus, we can interpret this as a breakdown of the polymer chain. Continued shearing has little further effect, though a slight increase in viscosity might be suspected due to eventual polymer coiling and entanglement.

We can conclude from Figure 12b that the apparatus design is sufficient to reproduce the expected polymer chain breakdown effect of ink jetting on polymer solutions, and thus gain confidence that the procedure can reasonably mimic the forces experienced by an ink during printing.

3.2 Changes in chemical content of latex binders

Figure 13 shows the effect that 20 passes through the syringe capillary has on the chemical makeup of the inkjet ink latices by comparing the FTIR spectra before and after the application of the extrusion (jetting) shear.

The loss of aromatic C-C and N-O after 20 passes (latex AP-600 K-1, dashed circles in Figure 13) through the high-shear regime could be indicative of the constituent styrene and/or species such as nitrosobenzene, which latter can act as a cross-linker during the polymerisation of the latex and/or for increasing strength on drying. Similarly, the loss of signal at ~720 cm^{-1} could relate to a loss of a species such as a hexamine moiety, typically added as a biocide preservative (latices L1 and L2, solid oval in Figure 13). No extra analyses were made to determine the exact nature of the species loss, but the fact that something becomes lost means that it becomes detached in some way from the main polymer into the surrounding liquid, and when the films are formed moves with the liquid (water) to the perimeters of the sample as evaporation proceeds, and thus are no longer present in the polymeric analysis.

3.3 Response of particle size, intrinsic viscosity and surface tension

The results from the designed process of repeated shear are sensitive to the three measured parameters:

(i) particle size, following changes according to the experimentally determined equivalent spherical diameter function ESD

$$esd_i = ESD(esd_{i-1}, \dot{\gamma}) \qquad [8]$$

where esd_i is the particle size after i passes exposed to a shear rate $\dot{\gamma}$, which is dependent on the previous value esd_{i-1},

(ii) intrinsic viscosity according to the following similar series function

$$\eta_i = H(\eta_{i-1}, \dot{\gamma}) \qquad [9]$$

where η_i, the intrinsic viscosity of the ink after i passes, is dependent on the previous viscous condition η_{i-1}, having been exposed to a shear rate of $\dot{\gamma}$, and

(iii) surface tension, similarly, as

$$\sigma_i = \Sigma(\sigma_{i-1}, \dot{\gamma}) \qquad [10]$$

The functions ESD, H and Σ thus describe the change in stability of the ink as a function of jetting. The starting values esd_0, η_0 and σ_0 are determined prior to the experiment. As we already saw in subsection 3.1, to a first approximation the function H for intrinsic viscosity of the PVOH polymer could be traced at least by eye following the dashed line shown. Should the
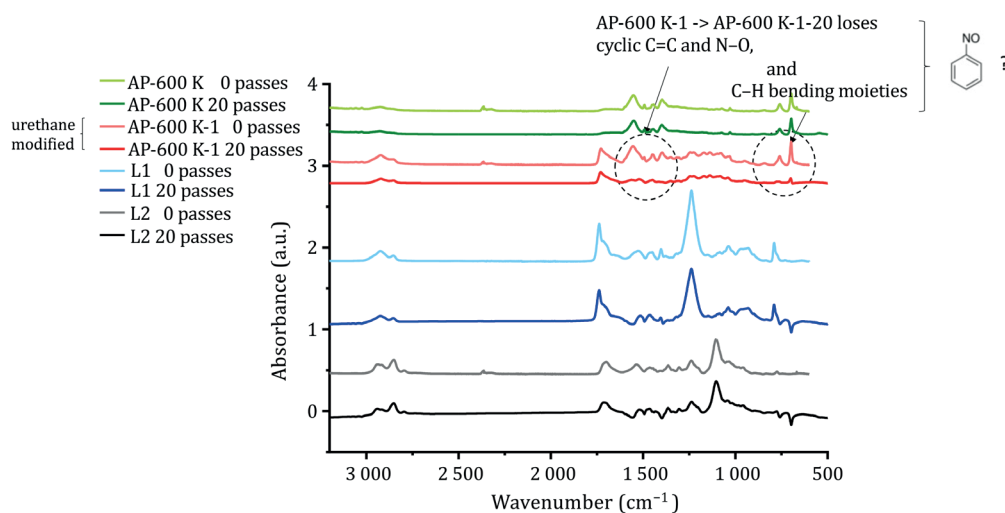

Figure 13: FTIR spectra of the four latex binders comparing the molecular constituents before and after the application of 20 passes through the repeated high shear mechanical syringe (jetting) regime; the units of absorbance are arbitrary and the stacked spectral plots are of comparable magnitude

procedure be used regularly in ink development, then similar experimental traces could be fitted for all three functions – we do not undertake this here since the sampling data are necessarily limited, due to sampling by hand, and would not yield fully reliable representations of the functions, however a fully developed procedure, perhaps a robotic process, would be able to support this approach.

We now report the sensitivity identified for the latex binders and inks in turn to the three parameters, including further observations of relevance.

3.3.1 Stability of latex binders

Figure 14 shows the ensemble averaged dynamic light scattering results of particle size (esd_i) for the AP-600 K and AP-600 K-1 latex pair tested for stability during increasing numbers of passes through the mechanical high shear capillary. We can see that there are a number of different responses. AP-600 K (Figure 14a) shows an initial reduction of a starting bimodal into a monomodal distribution, indicative of coagulation, followed by some agglomeration forming large particle sizes as a function of shearing. The reduction to monomodal and increase in size across the logarithmic scale suggests firstly cascade-type joining (coagulation) of particles, initially from 5 nm – so small as to be probably monomer or oligomer residue only – to 10 nm and onward to ~20 nm, and then to an equilibrium between agglomerate building and agglomerate breakdown under high shear at around ~130 nm, with some very large agglomerates building to ~5 000–6 000 nm (5–6 μm). Such large agglomerates could be prime suspects for inkjet nozzle blocking. After 40 passes, however, the large aggregates become broken down again and the size distribution reverts to a single peak a decade finer in size. AP-600 K-1 (Figure 14b), the urethane modified latex, essentially continues to display a strongly discrete bimodal particle size with a progressive transfer of particle occupancy from the coarser branch of the distribution to the finer as a function of progressive repeated shearing, being, interestingly, once again about a decade in size apart.
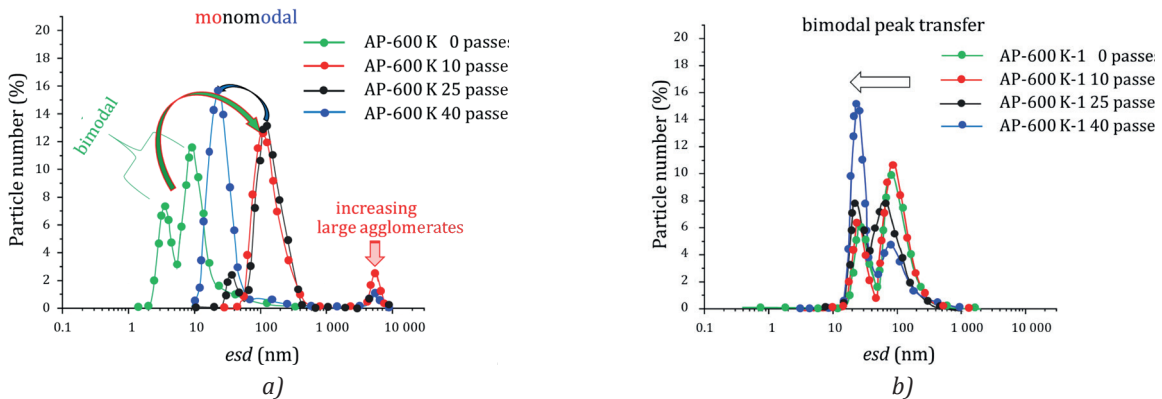

Figure 14: Particle size response, esd_i, of latices (a) AP-600 K, and (b) AP-600 K-1 (urethane modified) to repeated passes through the mechanical syringe at high shear
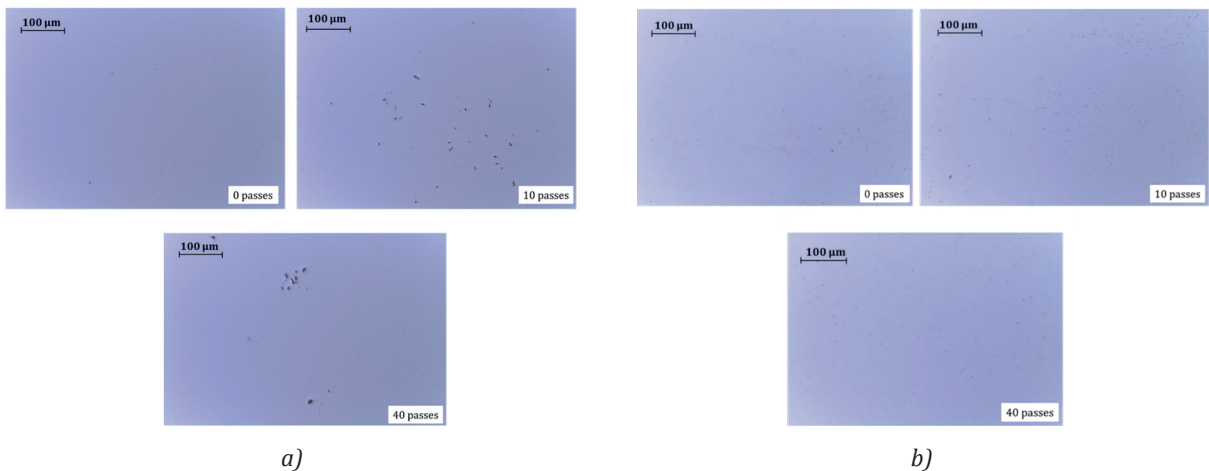

Figure 15: Optical microscopy of the latex suspensions following the formation of agglomerates as a function of number of passes through the mechanical syringe: (a) AP-600 K, (b) AP-600 K-1 (urethane modified)

Furthermore, we see in Figure 14 that the modification that was made to the latex AP-600 K-1 by adding the urethane moiety has apparently stabilised the latex particles against forming large aggregates. If we refer back to the FTIR spectrum for this latex in Figure 13 we saw that apparently a species becomes lost during repeated shearing. It was speculated that it might be a cross-linking agent. The modification appears to have released this species from the main polymer, and as a result the latex remains significantly more stable against aggregation or flocculation. Additionally, the change in size occupancy might also be related to a breakdown of the polymer cross-linking mechanism (Song and Winnik, 2005).

The agglomeration tendency can be followed physically using optical microscopy of the latex suspensions, Figure 15. The particle sizes observed correspond to the larger particle agglomerates in the light scattering size distribution data in Figures 14a and 14b. The optical resolution limit of ~0.25 μm limits the microscopic observation to random clusters/agglomerates only.

In contrast, in Figure 16, the two latices L1 and L2 show different behaviour as a function of multiple shearing.

The L1, on the one hand, remains quite stable against shear, but at a much larger particle size of ~50 nm, although with the appearance of a smaller size peak after 40 passes at ~12 nm. The L2, on the other hand, shows an initial reduction in particle size, suggesting separation of particles. Noting again the logarithmic scale of particle size (*esd*), the data suggest that the action of shearing on L2 is to break down a likely starting pair-wise particle-particle structure into single particles, i.e. from ~26 nm down to ~13 nm.
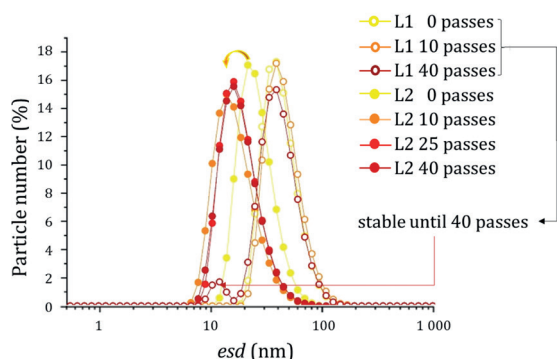

Figure 16: Particle size, esdᵢ, response of latices L1 and L2 to repeated passes through the mechanical syringe at high shear

The intrinsic viscosity of the latex suspensions is shown in Figure 17, in which it is clear to see that the particle volume flow properties at low shear remain similar for the AP-600 K and the L1 and L2 latices, whereas the urethane modified AP-600 K-1 has a distinctly lower viscosity flow, which may relate to the change in free additive content as seen previously in respect to particle size stability. We may conclude that the presence of a low number of agglomerates is not affecting the intrinsic viscosity. This is a very important finding in that it would be unlikely to identify a runnability problem in an inkjet component simply by considering viscosity measured using a typical printer's viscometer tool.
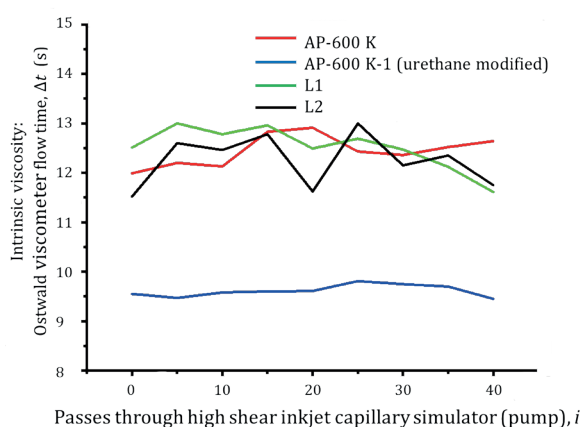

Figure 17: Intrinsic Ostwald viscometer flow time Δt (∝ η_i) for the four example latices

The surface tension results for the four latices are shown in Table 3. All the samples were measured at a consistent solids content of 5 g·dm⁻³. The values appear to be very similar except for the latex L1, which shows a higher surface tension – nonetheless relatively low when compared with the much higher surface tension of water, 75 mN·m⁻¹ – suggesting that this dispersion probably has less surfactant present, though still an effective amount. The analysis does not deliver any information concerning the hydrophilic nature of the latex particles themselves as the surface tension relates purely to the liquid solution phase only. We also can conclude that the wetting behaviour of the suspension remains constant irrespective of the repeated shearing experienced.

Table 3: Surface tension, σ_i (mN·m⁻¹), of the latex suspensions

| Latex | Number of passes through mechanical capillary, *i* | | |
	0	10	40
AP-600 K	43.26 ± 0.12	42.49 ± 0.17	42.33 ± 0.10
AP-600 K-1	37.44 ± 0.03	38.11 ± 0.02	37.56 ± 0.04
L1	58.73 ± 0.70	59.37 ± 0.07	59.27 ± 0.02
L2	42.17 ± 0.60	41.94 ± 0.20	42.23 ± 0.10

3.3.2 Inks

Having studied the challenging latex binder component found in many pigmented inks, we now consider the complete pigment formulated inks A (containing latex L1), B (containing latex L2) and R ("reference").

The starting "day zero" size distributions are shown in Figure 18, and the averaged data show that all the inks look alike and fall within the typical size range for a pigmented inkjet ink.
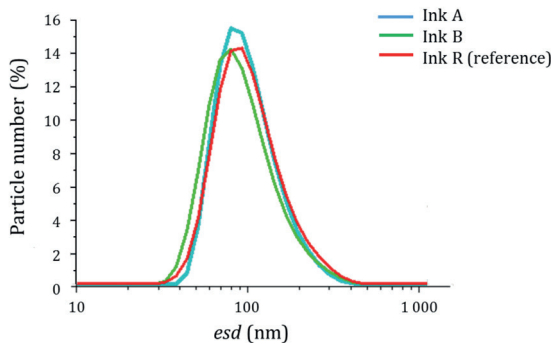

Figure 18: Starting "day zero" particle size distributions of the three inks

The impact of repeated applications of high shear in the mechanical syringe capillary are revealed for the three inks in Figure 19. In all cases the particle size of the contents decreases as a function of passes through the constant flow rate capillary.

Inks A and B behave very similarly, and, as is to be expected across the logarithmic scale in size (Figure 19), while the material becomes either broken down finer or increasingly dispersed, the particle size distribution broadens. This is typical of a grinding/milling process in which hard elastic, and brittle or softer particles coexist, in that the initial close to log-normal distribution becomes progressively skewed to the finer end as the more brittle or softer material grinds preferentially.

If we study the electron microscope images in Figure 20, taken from dried ink films using a field emission scanning electron microscope (FESEM) (Zeiss Sigma VP, Germany), we can notice three effects: (i) in all inks the particle material becomes finer as the number of passes under high shear increases, (ii) aggregates begin to appear as a function of repeated jetting, especially in inks A and B, and (iii) the ink R ("reference") appears not to have a film-forming binder, such as latex, and, as such, is better described as a pigment-only ink, as we see the pigment particles cluster into a random clumped powder distribution during the drying. This clustering is probably related to the "self-binding" design of ink, where the pigment

dispersant doubles up as a binder between them on drying, and this, at least partly, explains the clustered form of pigment distribution seen in the micrographs.
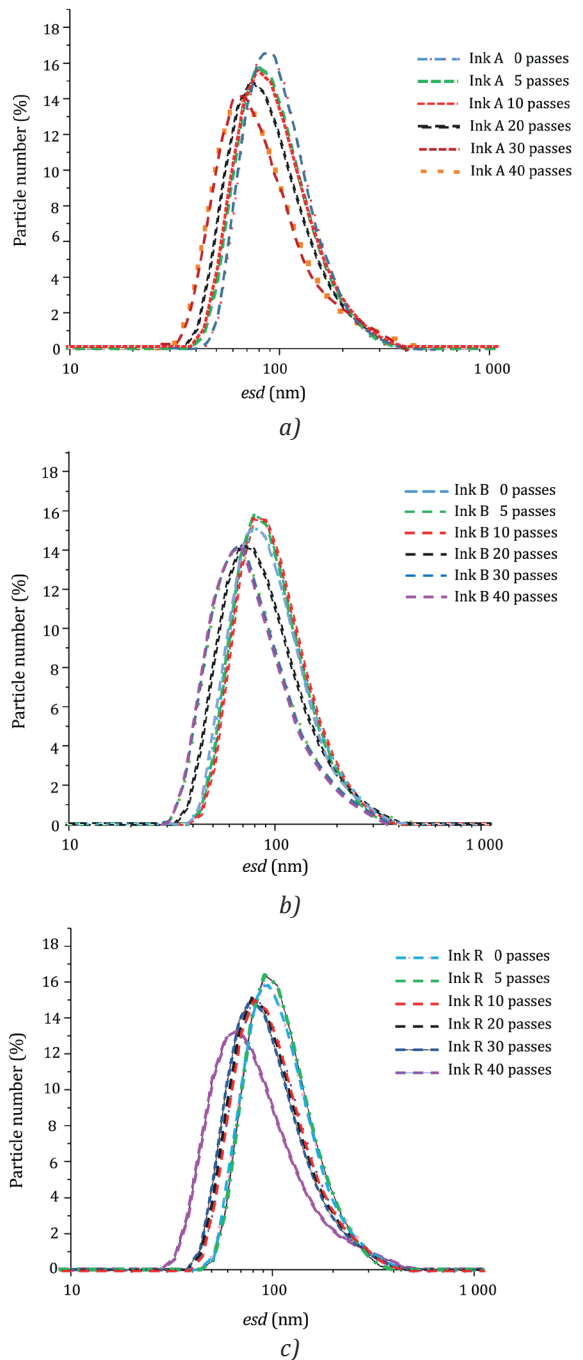

a)

b)

c)

Figure 19: Particle size distribution response to repeated shear through the mechanical capillary; (a) ink A with latex L1, (b) ink B with latex L2, and (c) ink R ("reference")

However, this allows us to make a further important observation since the particle size also becomes finer in ink R, strongly supporting the likelihood of pigment milling continuing during repeated jetting.
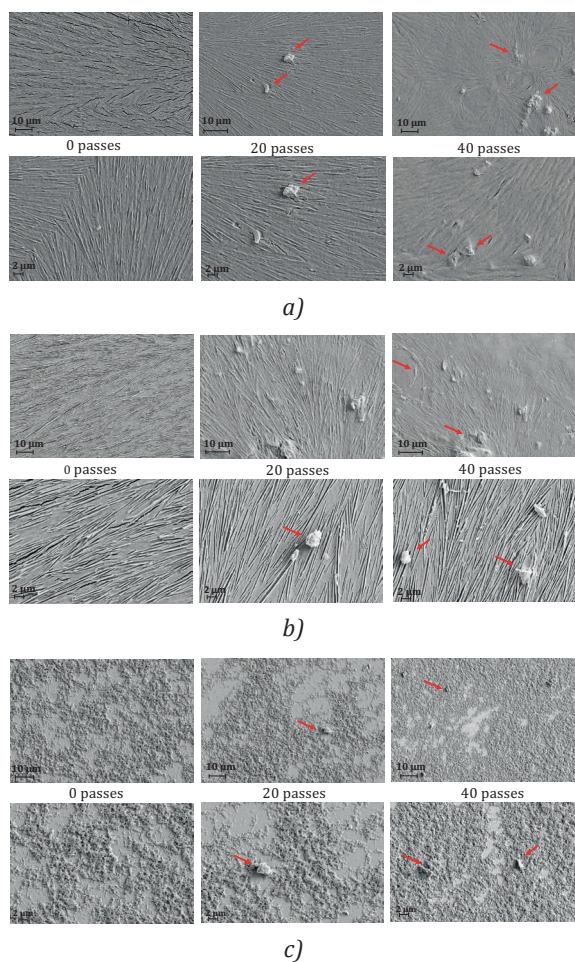
a)

b)

c)

Figure 20: Electron microscope images (FESEM, accelerating voltage 15 kV) of the three inks following the response to repeated exposure to shearing; (a) ink A, (b) ink B, and (c) ink R – the arrows indicate the formation of agglomerates

If pigment continues to be milled in this way in continuous inkjet printing, it will result in increased freshly formed pigment surface area, which, in turn, will adsorb free polymeric material, including excess stabilising dispersant. However, if this continues to a great extent, any excess dispersant will be consumed, such that the freshly milled pigment may not long remain stabilised in colloidal suspension and will flocculate in the stationary state or undergo shear-induced aggregation during jetting. Furthermore, removal of excess dispersant in this way will likely reduce the buffer capacity of the ink against any acidic attack, such as from the action of anaerobic bacteria. Apart from the question of colloidal stability, there might well be expected to be a change in print density and shade. This is clearly a topic for further work.

In the case of a complete ink, such as in A and B, there is a combination of pigment and latex. For example, ink B

has a magenta pigment, typically either dimethylquinacridone or dichloroquinacridone, according to the pigment colorant coding PR122 and PR202, respectively, having the formula
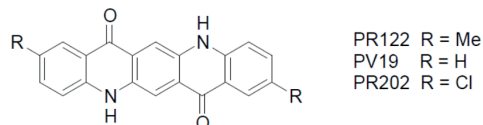
where the radical positions R are either unsubstituted hydrogen (H) (defined by the pigment colorant code PV19), methyl (CH_3) or chlorine (Cl). By studying the atomic elemental content using XPS method, it is possible to see if the pigment is concentrating also in the observed aggregates leading to changes in nitrogen, oxygen or chlorine levels. XPS is a surface sensitive technique and does not probe the bulk of the sample due to the material capture of emitted electrons. Thus, if a latex agglomerate were to occur it is likely that the outer surface would then be coated with pigment. Table 4 shows the comparative analysis of the unsheared ink B and an agglomerate formed after 20 passes through the mechanical capillary.

Table 4: Elemental analysis using XPS of ink B "day zero" (unsheared) versus an agglomerate structure

Ink B	0 passes		20 passes	
Element	Mass (%)	Atomic (%)	Mass (%)	Atomic (%)
N	22.47	25.08	18.08	10.72
O	75.91	74.20	76.61	76.88
Cl	1.62	0.71	5.31	2.40
total	100.00	100.00	100.00	100.00

From the elemental data in Table 4, we can immediately observe the large increase in chlorine (Cl) content, while the nitrogen content reduces, which is probably indicative of a surface concentration of pigment around the aggregate. It is not possible to determine whether the whole aggregate consists of pigment alone, but given the latex agglomeration tendency during shearing it is more likely that an ink containing such agglomerates would concentrate free pigment as a coating on such a sticky material. This is typical, incidentally, of the behaviour of latex binder stickies in papermaking, where the sticky agglomerate is covered by a mineral as a means of preventing the stickies from depositing on the papermachine. The minerals frequently used are either hydrophobic talc or bentonite/montmorillonite nanoclay (Benecke, et al., 2009; Gantenbein, et al., 2009; 2010; Gribble, et al., 2010; 2011).

The observed milling process is also seen in the intrinsic viscosity response, Figure 21, where progressive shearing leads to a steady decrease in passage time

P.A.C. Gane, et al. – J. Print Media Technol. Res. – Vol. 10 No. 1 (2021), 7–24

21

through the Ostwald viscometer. Once again we can note the unusual nature of "ink" R, which also, by these data, suggests it is predominantly pigment only.
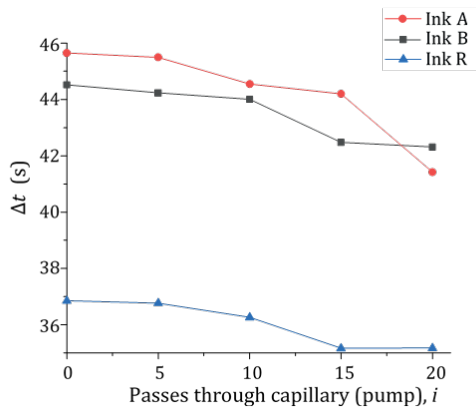

Figure 21: Displaying the steady drop in intrinsic viscosity (passage time through the Ostwald viscometer) as a function of passes through the mechanical syringe capillary

As in the case of the latices, the surface tension values for the inks, Table 5, measured at a solids content of 1 g·dm⁻³, remain stable also through the shearing process, and lie between the lower and upper latex values, suggesting the presence of a certain amount of surfactant to aid wetting during printing.

Table 5: Surface tension, σ_i (mN·m⁻¹), of the inkjet inks

Ink	Number of passes through mechanical capillary, i		
	0	10	40
A	49.94 ± 0.06	49.61 ± 0.05	50.24 ± 0.12
B	50.31 ± 0.09	49.63 ± 0.07	49.67 ± 0.02
R (ref.)	48.41 ± 0.01	49.45 ± 0.08	49.75 ± 0.04

3.3.3 Jettability

The response in respect to particle size is seen as the most critical aspect found in this study, and is logical when considering the challenges of inkjet printing centre almost solely on the behaviour of the ink at the jetting nozzle. The presence of agglomerates or dried material lead to failure of the jet with either reduced droplet ink amount, usually accompanied by distortion of the droplet trajectory, or complete absence of ink altogether. Plate wetting and spreading of ink around the nozzle can also lead to disturbance of the break-away of ink from the printhead. This latter can either be due to problems of surface tension, which interestingly we did not see, or more likely in the light of our results capillarity across the surface of any dry build-up of ink or deposition of agglomerates around the nozzle exit.

Given the focus on agglomeration, it is worth taking a reality check on dimensions. Amongst the latices tested we saw particle sizes ranging from 5 nm to 200 nm. Suppose a printer desires two settings for certain jobs, e.g. 1 pl for the finest functional technical work, including, say, printed electronics, and 1 μl for general book and standard image printing. If we convert these liquid volumes to physical droplet diameters then they are equivalent to $\sqrt[3]{6/\pi \times 10^{-15}} \approx 1.2 \times 10^{-5}$ m and $\sqrt[3]{6/\pi \times 10^{-9}} \approx 1.2 \times 10^{-3}$ m, respectively. In respect to latex size, at least 200–300 spheres of 100 nm diameter could fit into a 1 pl droplet, and as many as 30 000–40 000 such spheres in a 1 μl droplet. However, agglomerates of 10 000 nm (10 μm), such as exhibited by the latex AP-600 K would block pl droplet generation and at least distort, if not also block by further build-up, the production of μl droplets. AP-600 K-1 (urethane modified) by contrast, with its bimodality, would be suitable for, say, down to > 100 pl, despite the particle size changes between the bimodal branches (actually getting finer), and L1 at ≤ 100 nm could be possible to use, like AK-66 K-1, in the upper pl range and certainly for μl droplet work, and their demonstrated stability against agglomeration should ensure satisfactory freedom of nozzle blocking provided no subsequently drying deposition around the nozzle exit occurred. Latex L2 after initial shear to disperse fully the "day zero" state, being then all ≤ 50 nm, should be well suitable for pl work.

As discussed in section 1. Introduction, there are a multitude of parameters, other than colloidal instability to shear, which control inkjet runnability, including the viscoelastic response to the displacement pulse magnitude and frequency in the printhead, exposure to air and drying at the nozzle exit, involving also air ingress during the displacement relaxation cycle, phase separation tendency leading to deposits at chamber walls, etc. Therefore, the novel test and supporting analyses proposed here address a subset, albeit a significant one, of the parameters affecting the dynamic response of the ink, especially particulate-containing ink, which, given the growing trend of using inkjet printing for patterning of functional inks, is increasing rapidly in relevance.

4. Conclusions

The evidence collected suggest that a constant flow rate mechanically driven syringe capillary device can induce the shear-related effects on both polymer and particle agglomerate breakdown as well as particle-particle aggregation via colloidal destabilisation. Such an opportunity to predict the constant flow rate shear-related runnability of inkjet ink in this way could provide a means of reducing on-machine trial time and avoidance of potentially expensive printhead damage.

The study of individual component parts of an ink-jet ink, such as latex binder and pigment, separately, reveals the stability of each against repeated jetting shear conditions. Latex is confirmed to be particularly susceptible to both phenomena, showing initial coagulation and agglomerate build, followed by equilibrium breakdown and rebuild of these structures after multiple shearing. In combination with pigment, compound agglomerates have been shown to form, and it is speculated, using elemental analysis, that latex coagulates become covered by pigment, much as sticky deposits in papermaking become covered with mineral particles.

Pigment is seen to undergo increased dispersion under initial shear, followed by a milling action during repeated shearing, such that the particle size progressively decreases.

Implications for jettability can be concluded, in that agglomerates are likely to induce nozzle blocking, and milling of pigment is expected to change subsequent print density and substrate coverage performance. It is hoped that using the novel device and procedure reported here, such effects can be readily studied in the future in combination with runnability prediction.

Acknowledgements

References

Alamán, J., Alicante, R., Peña, J.I. and Sánchez-Somolinos, C., 2016. Inkjet printing of functional materials for optical and photonic applications. *Materials*, 9(11): 910. https://doi.org/10.3390/ma9110910.

Beedasy, V. and Smith, P.J., 2020. Printed electronics as prepared by inkjet printing. *Materials,* 13(3): 704. https://doi.org/10.3390/ma13030704.

Benecke, F., Gantenbein, D., Schoelkopf, J., Gane, P.A.C. and Gliese, T., 2009. Organic contaminants in recycled paper: a model study of the adsorbent properties of talc for idealised component suspensions. *Nordic Pulp and Paper Research Journal*, 24(2), pp. 219–224. https://doi.org/10.3183/npprj-2009-24-02-p219-224.

Biswas, T.T., Yu, J. and Nierstrasz, V.A., 2019. Effects of ink characteristics and piezo-electric inkjetting parameters on lysozyme activity. *Scientific Reports,* 9: 18252. https://doi.org/10.1038/s41598-019-54723-9.

Cui, X., Boland, T., D'Lima, D.D. and Lotz, M.K., 2012. Thermal inkjet printing in tissue engineering and regenerative medicine. *Recent Patents on Drug Delivery & Formulation*, 6(2), pp. 149–155. https://doi.org/10.2174/187221112800672949.

Cui, X., Gao, G., Yonezawa, T. and Dai, G., 2014. Human cartilage tissue fabrication using three-dimensional inkjet printing technology. *Journal of Visualized Experiments,* 88: e51294. https://doi.org/10.3791/51294.

Ebert, J., Özkol, E., Zeichner, A., Uibel, K., Weiss, Ö., Koops, U., Telle, R. and Fischer, H., 2009. Direct inkjet printing of dental prostheses made of zirconia. *Journal of Dental Research*, 88(7), pp. 673–676. https://doi.org/10.1177/0022034509339988.

Eggenhuisen, T.M., Galagan, Y., Biezemans, A.F.K.V., Slaats, T.M.W.L., Voorthuijzen, W.P., Kommeren, S., Shanmugam, S., Teunissen, J.P., Hadipour, A., Verhees, W.J.H., Veenstra, S.C., Coenen, M.J.J., Gilot, J., Andriessen, R. and Groen W.A., 2015. High efficiency, fully inkjet printed organic solar cells with freedom of design. *Journal of Materials Chemistry A*, 3(14), pp. 7255–7262. https://doi.org/10.1039/C5TA00540J.

Gantenbein, D., Schoelkopf, J., Gane, P.A.C. and Matthews, G.P., 2010. Influence of pH on the adsorption of dissolved and colloidal substances in a thermo-mechanical pulp filtrate onto talc. *Nordic Pulp and Paper Research Journal*, 25(3), pp. 288–299. https://doi.org/10.3183/npprj-2010-25-03-p288-299.

Gantenbein, D., Schoelkopf, J., Hunziker, P., Matthews, G.P. and Gane, P.A.C., 2009. Efficiency of colloidal pitch adsorption onto phyllosilicates: comparing talc, chlorite and pyrophyllite. *Nordic Pulp and Paper Research* Journal, 24(4), pp. 448–458. https://doi.org/10.3183/npprj-2009-24-04-p448-458.

Gao, M., Li, L. and Song, Y., 2017. Inkjet printing wearable electronic devices. *Journal of Materials Chemistry C*, 5(12), pp. 2971–2993. https://doi.org/10.1039/C7TC00038C.

Gribble, C.M, Matthews, G.P., Turner, A., Gantenbein, D., Schoelkopf, J. and Gane, P.A.C., 2011. Equilibrium coefficients for the adsorption of colloidal stickies onto mineral suspension particulates to improve paper recycling. *Nordic Pulp and Paper Research Journal*, 26(4), pp. 421–427. https://doi.org/10.3183/npprj-2011-26-04-p421-428.

Gribble, C.M., Matthews, G.P., Gantenbein, D., Turner, A., Schoelkopf, J. and Gane, P.A.C., 2010. Adsorption of surfactant-rich stickies onto mineral surfaces. *Journal of Colloid and Interface Science*, 352(2), pp. 483–490. https://doi.org/10.1016/j.jcis.2010.07.062.

P.A.C. Gane, et al. – J. Print Media Technol. Res. – Vol. 10 No. 1 (2021), 7–24

23

Hoath, S.D., Martin, G.D., Tuladhar, T.R., Mackley, M.R., Hutchings, I.M. and Vadillo, D.C., 2009. Links between ink rheology, drop-on-demand jet formation, and printability. *Journal of Imaging Science and Technology*, 53(4): 041208. https://doi.org/10.2352/J.ImagingSci.Technol.2009.53.4.041208.

Jiang, X., Li, W., Hai, T., Yue, R., Chen, Z., Lao, C., Ge, Y., Xie, G., Wen, Q. and Zhang, H., 2019. Inkjet-printed MXene micro-scale devices for integrated broadband ultrafast photonics. *2D Materials and Applications*, 3: 34. https://doi.org/10.1038/s41699-019-0117-3.

Jutila, E., Koivunen, R., Bollström, R. and Gane, P., 2015. Thin layer chromatographic behaviour of dyes during microfluidic transport in functionalised calcium carbonate coatings. In: P. Gane, ed. *Advances in Printing and Media Technology: Proceedings of the 42nd International Research Conference of iarigai*. Helsinki, Finland, 06–09 September 2015. Darmstadt, Germany: iarigai, pp. 255–264.

Jutila, E., Koivunen, R., Bollström, R. and Gane, P., 2020. Fully inkjet-printed glucose assay fabricated on highly porous pigment coating. *Microfluidics and Nanofluidics*, 24(6): 40. https://doi.org/10.1007/s10404-020-02344-4.

Jutila, E., Koivunen, R., Kiiski, I., Bollström, R., Sikanen, T. and Gane, P., 2018. Microfluidic lateral flow cytochrome P450 assay on a novel printed functionalized calcium carbonate-based platform for rapid screening of human xenobiotic metabolism. *Advanced Functional Materials*, 28(31): 1802793. https://doi.org//10.1002/adfm.201802793.

Kim, H.S., Kang, J.S., Park, J.S., Hahn, H.T., Jung, H.C. and Joung, J.W., 2009. Inkjet printed electronics for multifunctional composite structure. *Composites Science and Technology*, 69(7–8), pp. 1256–1264. https://doi.org/10.1016/j.compscitech.2009.02.034.

Koivunen, R., Jutila, E. and Gane, P., 2015. Inkjet printed hydrophobic microfluidic channelling on porous substrates. *Journal of Print and Media Technology Research*, 4(1), pp. 7–17. https://doi.org/10.14622/JPMTR-1413.

Koivunen, R., Jutila, E., Bollström, R. and Gane, P., 2016. Hydrophobic patterning of functional porous pigment coatings by inkjet printing. *Microfluidics and Nanofluidics*, 20(6): 83. https://doi.org/10.1007/s10404-016-1747-9.

Koivunen, R., Jutila, E., Bollström, R. and Gane, P., 2017. Inkjet printed polyelectrolyte patterns for analyte separation on inherently porous microfluidic analytical designs. *Colloids and Surfaces A: Physicochemical and Engineering Aspects*, 522, pp. 218–232. https://doi.org/10.1016/j.colsurfa.2017.03.001.

Koivunen, R., Jutila, E., Bollström, R. and Gane, P., 2019. Investigating chromatographic interactions in porous pigment coatings between inkjettable polyelectrolytes and model colorant solutions. *Colloids and Surfaces A: Physicochemical and Engineering Aspects*, 579: 123676. https://doi.org/10.1016/j.colsurfa.2019.123676.

Krainer, S., Smit, C. and Hirn, U., 2019. The effect of viscosity and surface tension on inkjet printed picoliter dots. *RSC Advances*, 9(54), pp. 31708–31719. https://doi.org/10.1039/C9RA04993B.

Lee, A., Sudau, K., Ahn, K.H., Lee, S.J. and Willenbacher, N., 2012. Optimization of experimental parameters to suppress nozzle clogging in inkjet printing. *Industrial & Engineering Chemistry Research*, 51(40), pp. 13195–13204. https://doi.org/10.1021/ie301403g.

Li, Y., Dahhan, O., Filipe, C.D.M., Brennan, J.D. and Pelton, R.H., 2019. Deposited nanoparticles can promote air clogging of piezoelectric inkjet printhead nozzles. *Langmuir*, 35(16), pp. 5517–5524. https://doi.org/10.1021/acs.langmuir.8b04335.

Matsusaki, M., Sakaue, K., Kadowaki, K. and Akashi, M., 2013. Three-dimensional human tissue chips fabricated by rapid and automatic inkjet cell printing. *Advanced Healthcare Materials*, 2(4), pp. 534–539. https://doi.org/10.1002/adhm.201200299.

Renner, J. and Bircher, F., 2017. Waveform optimization for piezo drop on demand inkjet printheads by meniscus motion analysis. In: P. Gane, ed. *Advances in Printing and Media Technology: Proceedings of the 44th International Research Conference of iarigai*. Fribourg, Switzerland, September 2017. Darmstadt, Germany: iarigai, pp. 15–20.

Saarinen, J.J., Valtakari, D., Haapanen, J., Salminen, T., Mäkelä, J.M. and Uozumi, J., 2014. Surface-enhanced Raman scattering active substrates by liquid flame spray deposited and inkjet printed silver nanoparticles. *Optical Review*, 21(3), pp. 339–344. https://doi.org/10.1007/s10043-014-0051-8.

Song, J.-S. and Winnik, M.A., 2005. Cross-linked, monodisperse, micron-sized polystyrene particles by two-stage dispersion polymerization. *Macromolecules*, 38(20), pp. 8300–8307. https://doi.org/10.1021/ma050992z.

Sumaiya, S., Kardel, K. and El-Shahat, A., 2017. Organic solar cell by inkjet orienting – an overview. *Technologies*, 5(3): 53. https://doi.org/10.3390/technologies5030053.

Tuladhar, T., 2017. Measurement of complex rheology and jettability of inkjet inks. In: W. Zapka, ed. *Handbook of industrial inkjet printing: a full system approach*. Weinheim, Germany: Wiley–VCH Verlag, Ch. 22. https://doi.org/10.1002/9783527687169.ch22.

Vadillo, D.C., Tuladhar, T.R., Mulji, A.C., Jung, S., Hoath, S.D. and Mackley, M.R., 2010a. Evaluation of the inkjet fluid's performance using "Cambridge Trimaster" filament stretch and break-up device. *Journal of Rheology*, 54(2), pp. 261–282. https://doi.org/10.1122/1.3302451.

Vadillo, D.C., Tuladhar, T.R., Mulji, A.C. and Mackley, M.R., 2010b. The rheological characterisation of linear viscoelasticity for ink jet fluids using piezo axial vibrator and torsion resonator rheometers. *Journal of Rheology*, 54(4), pp. 781–795. https://doi.org/10.1122/1.3439696.

Wheeler, J.S.R., Reynolds, S.W., Lancaster, S., Romanguera, V.S. and Yeates, S.G., 2014. Polymer degradation during continuous ink-jet printing. *Polymer Degradation and Stability*, 105, pp. 116–121. https://doi.org/10.1016/j.polymdegradstab.2014.04.007.

Whorlow, R.W., 1992. *Rheological techniques*. New York, NY, USA: Ellis Horwood.

Yokoi, K., Vadillo, D., Hinch, J. and Hutchings, I., 2009. Numerical studies of the influence of the dynamic contact angle on a droplet impacting on a dry surface. *Physics of Fluids*, 21(7): 072102. https://doi.org/10.1063/1.3158468.

Zönnchen, N., Wenger, R., Mauron, M. and Bircher, F., 2019. Bioprinting of thick, vascularized tissues by inkjet-technology. In: C. Ridgway, ed. *Advances in Printing and Media Technology: Proceedings of the 46th International Research Conference of iarigai*. Stuttgart, Germany, 15–18 September 2019. Darmstadt, Germany: iarigai, pp. 105–115.